

Dynamic carrier distribution in quantum wells modulated by surface acoustic waves

F. Alsina,* P. V. Santos, and R. Hey

Paul-Drude-Institut für Festkörperelektronik, Hausvogteiplatz 5-7, 10117 Berlin, Germany

A. García-Cristóbal and A. Cantarero

Materials Science Institute, Universitat de València, Burjassot, E-46100 València, Spain

(Received 12 March 2001; published 28 June 2001)

We have investigated the dynamics of photogenerated carriers under surface acoustic wave (SAW) fields in GaAs quantum wells using spatially and time-resolved photoluminescence (PL). The frequency and phase of the PL oscillations under a SAW yield information about the carrier distribution and the band-gap modulation induced by the SAW. We directly prove that the transport properties of the carriers ultimately control their distribution, storage and, subsequent recombination in the modulated potential.

DOI: 10.1103/PhysRevB.64.041304

PACS number(s): 77.65.Dq, 77.65.Ly, 78.47.+p, 78.55.-m

The periodic modulation of the optical properties induced by a surface acoustic wave (SAW) has been traditionally used to control the intensity and the propagation direction of light beams in piezoelectric insulators. In polar semiconductors, the piezoelectric field of the SAW interacts strongly with carriers, thus opening the possibility of using these waves to induce a dynamic lateral modulation of the electronic properties. In addition to the strong type-II modulation imposed by the piezoelectric field, the strain field of the SAW leads to a weak lateral modulation of the band gap. The SAW fields have been applied to control the lifetime and the transport of photogenerated carriers and of their spins in low-dimensional semiconductor structures.¹⁻³ In these applications, the SAW piezoelectric field ionizes photogenerated electron-hole pairs. The free electrons and holes are then trapped in the region of maxima and minima of the moving piezoelectric potential. The spatial separation considerably increases the carrier lifetime, so that they can be transported over macroscopic distances by the SAW.²

An interesting question regarding the interaction between SAW's and photogenerated carriers is how the latter distribute in the dynamic strain and piezoelectric fields, when the SAW wavelength λ_{SAW} and oscillation frequency ω_{SAW} become comparable to the carrier transport lengths and inverse lifetimes, respectively. In this work, we investigate the carrier dynamics in GaAs quantum wells (QW's) under high-frequency SAW's using time-resolved and spatially resolved photoluminescence (PL) spectroscopy. Since the modulation introduced by SAW's is both spatial and time dependent, this technique gives a deep insight into the mechanisms of the interaction between SAW's and carriers. We demonstrate that the modulation of the optical properties by high-frequency SAW's is dominated by nonlocal effects in time and space arising from the dynamic redistribution of photoexcited carriers in the SAW profile. In fact, while for low SAW frequencies the probability of ionization of electron-hole pairs by the piezoelectric field is expected to depend only on the magnitude of the field, and thus to be modulated only at multiples of ω_{SAW} , the measured PL under a high-frequency SAW displays a strong modulation at the fundamental frequency ω_{SAW} . This behavior is explained by taking into account the transport properties of the

photogenerated carriers and their ability to follow the moving potential. Furthermore, we show that the intensity, energy, and phase of the PL pulses provide a direct mapping of the microscopic carrier distribution and of the band-gap modulation induced by the SAW.

The studies were performed on a 15-nm GaAs QW with $\text{Al}_{0.3}\text{Ga}_{0.7}\text{As}$ barriers grown by molecular-beam epitaxy on GaAs (001). The QW is placed 200 nm below the surface. SAW's propagating along the $x=[110]$ surface direction were generated by aluminum split-finger interdigital transducers (IDT's) deposited on the sample surface and designed for operation at a wavelength $\lambda_{\text{SAW}}=5.6 \mu\text{m}$ [corresponding to a frequency $\omega_{\text{SAW}}/(2\pi)=520 \text{ MHz}$ at 12 K]. The PL measurements were carried out at 12 K using a confocal microscope with illumination and detection areas with a diameter of about $2 \mu\text{m}$. The continuous radiation from a Ti:sapphire laser ($\lambda_L=765 \text{ nm}$) was employed as excitation source. Time resolution was achieved by using a fast photomultiplier (time resolution of approximately 0.4 ns) to detect the PL. Information about the SAW phase was obtained by synchronizing the photomultiplier with the radio-frequency (rf) generator employed to drive the IDT's. The setup also allows for interferometric measurements of the surface displacement u_z induced by the SAW, which was used to determine the amplitude of the SAW strain field.

The effects of the SAW fields on the cw PL are illustrated in Fig. 1(a). The spectra were recorded with coincident illumination and detection areas in the absence (line) and under the influence of a SAW with a nominal excitation power of 16 dBm (dots). In the latter case, the PL intensity becomes strongly suppressed due to the interaction between the SAW piezoelectric field and the photogenerated carriers.¹⁻³ In addition, the PL line exhibits a small blueshift, which arises from the SAW strain field, as will be demonstrated in the following.

The dynamics of the PL quenching becomes apparent in time-resolved measurements. Figure 2(a) shows the PL traces collected at 1.5331 eV, which coincides with the maximum of the spectrum for $P_{\text{rf}}=16 \text{ dBm}$ in Fig. 1(a). The PL signal is time modulated with the periodicity $T_{\text{SAW}}=2\pi/\omega_{\text{SAW}}=1.92 \text{ ns}$ of the applied SAW. The modulation is superimposed on a background, leading to a modulation

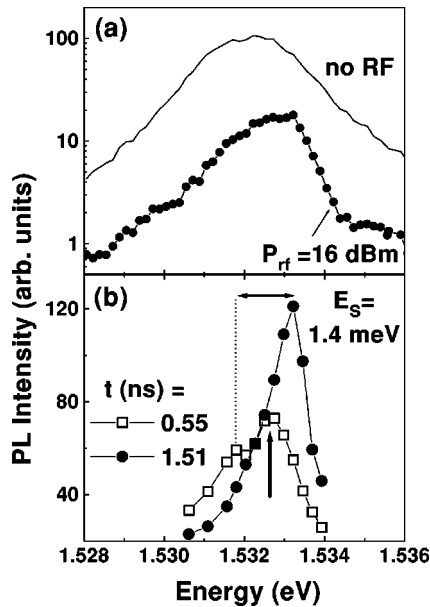


FIG. 1. (a) PL spectra (semilogarithmic plot) of a 15-nm GaAs/Al_{0.3}Ga_{0.7}As single QW in the absence (line) and under the influence of a surface acoustic wave with $P_{\text{rf}}=16$ dBm (line with dots). (b) PL intensity obtained from Fig. 5 at $t_{\text{min}}=0.55$ ns and $t_{\text{max}}=1.51$ ns.

amplitude of approximately 50% of the mean PL value. The latter decreases with the rf power (not shown) in agreement with the time-integrated PL spectra displayed in Fig. 1(a). We can rule out effects other than the interaction with the SAW as the source of the reported changes, since (i) the oscillations in the time-resolved signal were observed on the SAW path in areas far away from the transducer, and (ii) they completely disappear, and the PL signal recovers the value without SAW, when the rf is detuned from the transducer resonance band.

The background superimposed on the oscillations is al-

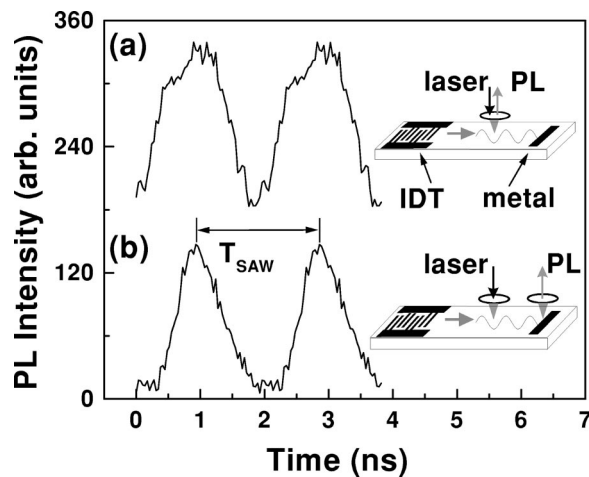


FIG. 2. Time-resolved PL measured at 1.5331 eV for (a) coincident and (b) spatially separated excitation and detection areas. In (b) the detection spot is placed 6 μm away from the excitation area along the SAW propagation direction. T_{SAW} denotes the SAW oscillation period.

most suppressed when the PL is recorded with spatially separated illumination and detection spots. The separation was achieved by displacing the detection pinhole in the PL setup away from its confocal position, following the procedure described in Ref. 4. Figure 2(b) displays a time-resolved PL trace recorded when the PL is detected 6 μm away from the generation position along the propagation direction of the SAW. The PL, in this case, arises from carriers that are transported by the SAW and recombine within the detection area. In order to enhance the carrier recombination, the detection spot was placed next to a semitransparent metal stripe used to quench the SAW piezoelectric field.⁵ The distantly detected PL is only observed when the rf is switched on, further evidencing that it is induced by the recombination of carriers transported by the SAW.

The ionization and spatial separation of electron-hole pairs is expected to be a nonlinear function of the SAW piezoelectric field, since it depends only on the magnitude and not on the sign of the field. As a consequence, the PL oscillations should be dominated by components at the second and higher harmonics of the SAW frequency ω_{SAW} . The experimental results in Fig. 2, however, show a strong modulation at the fundamental frequency ω_{SAW} . The discrepancy is attributed to the fundamental role of the carrier transport properties on the modulation mechanism. In order to clarify this point, we performed simulations of the carrier distribution and of the recombination probability in the dynamic SAW profile. In a first step, the strain field and the strain-induced energy changes of the conduction (CB) and valence bands (VB) were calculated following the method described in Ref. 5. The amplitude of the SAW fields was determined by adjusting the SAW vertical displacement field (u_z) obtained from an elastic model⁶ to the value obtained by interferometry [symbols in Fig. 3(a)]. The calculated strain-induced shifts of the electron (ΔE_e) and heavy-hole (ΔE_{hh}) energy levels are displayed in Fig. 3(b). In a second step, the carrier distribution in the modulated conduction and valence bands, as well as the recombination rate, were calculated by solving the drift-diffusion equations for electrons and holes in the SAW potential.

Figures 4(a–c) display spatial profiles for the electron (n , solid line) and hole (p , dashed line) densities, the recombination probability ($\propto np$, dots), as well as the piezoelectric potential (Φ), for three successive times. In the calculations, we assumed that the carriers are continuously generated in the dashed region around $x=0$ starting at time $t=0$. Electron (μ_e) and hole (μ_h) mobilities of 5000 and 500 $\text{cm}^2/(\text{V s})$, respectively, were used in the simulations. The same qualitative results were obtained for carrier mobilities in a wide range around these values, as long as $\mu_e \gg \mu_h$. As time progresses, the carriers are swept along the SAW propagation direction. The concentration profiles away from the generation area can be easily understood by considering that, in order to follow the dynamic modulation induced by the SAW, the mobilities μ_e and μ_h must exceed $v_{\text{SAW}}/F_{\text{eff}}$, where v_{SAW} denotes the SAW propagation velocity and $F_{\text{eff}} = |\partial\Phi/\partial x'|_{\text{max}}$ the effective field created by the modulated potential profile Φ . This condition is normally satisfied for the highly mobile electrons, which display a sharp spatial

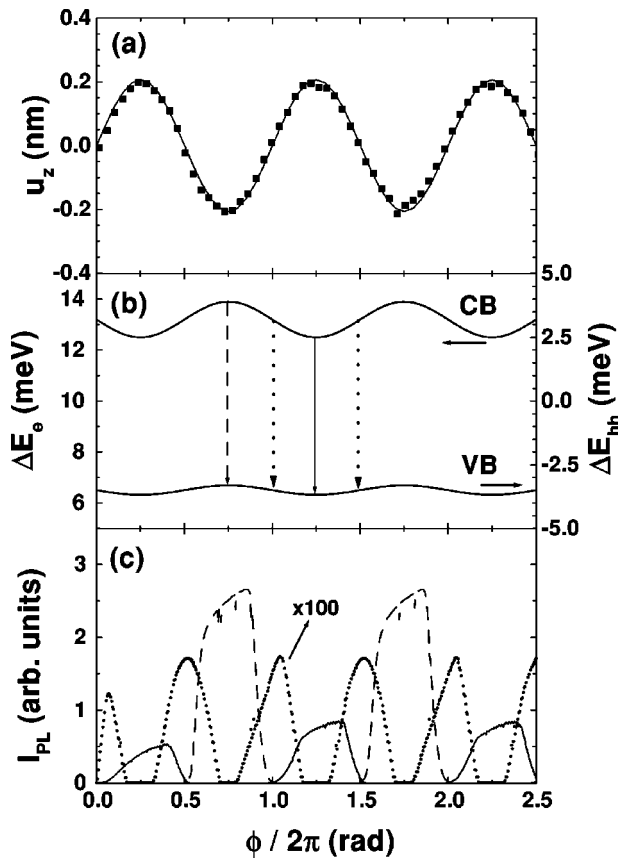


FIG. 3. (a) Measured (square dots) and calculated (solid line) surface displacement u_z for a SAW with $P_{\text{rf}}=16$ dBm as a function of the SAW phase $\phi=(2\pi/\lambda_{\text{SAW}})x-\omega_{\text{SAW}}t$. (b) Calculated conduction (CB, ΔE_e) and valence band (VB, ΔE_{hh}) modulation induced by the SAW strain. (c) Calculated PL intensity (I_{PL}) at the three energies depicted by the vertical arrows in (b).

distribution around the potential maxima. The holes, however, are less able to follow the dynamic modulation. As a consequence, they show a much wider spatial distribution in the SAW field as compared to electrons (cf. Fig. 4). Therefore, the spatial distribution of the recombination probability, proportional to np , basically reflects that of the electron distribution n . In agreement with Fig. 2(b), PL pulses appear once within an rf cycle, when the maximum in the electron density crosses the detection point at a fixed position away from the generation area.

The asymmetry in mobilities for electrons and holes also accounts for the time dependence of the PL emission for confocal generation and detection at position $x=0$. The continuous carrier generation makes the profiles more complex in this case. When the potential is maximum in the generation area [cf. Fig. 4(a)], photogenerated electrons are kept around $x=0$. The low mobility of the holes, however, restricts their ability to reach regions of minimum potential, leading to a maximum recombination probability. The situation reverses when the SAW potential reaches a minimum [Fig. 4(c)], since electrons can be quickly extracted from the generation area before substantial recombination occurs. The decrease in the recombination rate leads to significant carrier storage in the modulated potential profile.

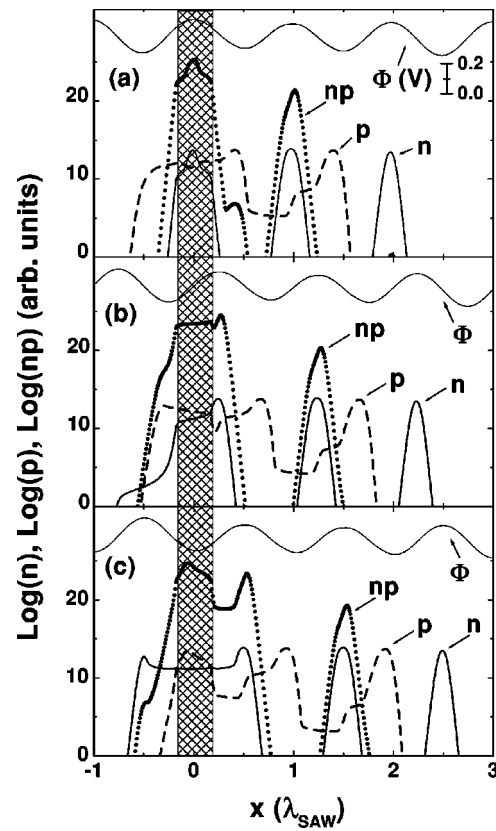


FIG. 4. Spatial dependence of the potential (Φ), the electron (n , solid lines) and hole p (dashed lines) concentrations, as well as the np -product (dots) calculated for three times corresponding to (a) maximum ($t=2 T_{\text{SAW}}$), (b) zero ($t=2.25 T_{\text{SAW}}$), and (c) minimum ($t=2.5 T_{\text{SAW}}$) values of the potential $\Phi(x=0)$, where T_{SAW} denotes the SAW period. The dashed region represents the illumination area.

The well-defined phase relation between the SAW strain and piezoelectric fields, which are responsible for the modulation of the band gap and of the carrier distribution, respectively, *correlates the intensity, energy, and phase* of the time-resolved PL pulses. This effect becomes clear in Fig. 3(c), which displays simulated time-resolved PL traces for confocal excitation and detection at the three transition energies indicated by vertical arrows in Fig. 3(b). When the detection energy corresponds to the maximum band gap ($E_{\text{g,max}}$, dashed line) or to the minimum band gap ($E_{\text{g,min}}$, solid line), only a single PL pulse per rf cycle is expected. The pulses are displaced in phase by 180° , since emission at these two energies takes place at time intervals differing by $T_{\text{SAW}}/2$ (the width of the simulated PL pulses are determined by the spatial extent of the illumination and detection areas indicated in Fig. 4). The PL modulation is the largest for detection at $E_{\text{g,max}}$ due to the reasons discussed in the previous paragraph. For detection energies between $E_{\text{g,min}}$ and $E_{\text{g,max}}$, two pulses per cycle are expected, when the band gap matches the detection energy. According to the calculations in Fig. 3(c), the intensity of the pulses is considerably smaller than in the previous cases due to the strong electric field.

As a consequence of the strain-induced band-gap modu-

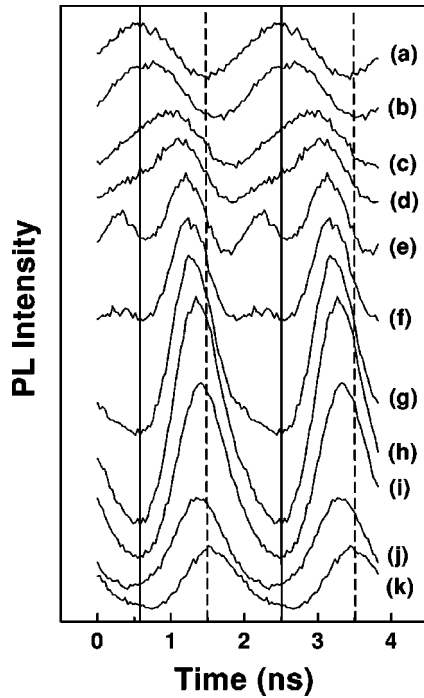


FIG. 5. Time-resolved PL detected at energies ranging from (a) 1.5316 eV to (k) 1.5339 eV in steps of 0.25 meV. Measurements were performed with coincident illumination and detection areas. For clarity, the curves are displaced vertically.

lation, the cw PL line splits under a SAW into a doublet with energy separation $E_s = E_{g,\max} - E_{g,\min}$ corresponding to the peak-to-peak amplitude of the band-gap modulation.⁵ The splitting is not observed in Fig. 1(a) due to the large width of the PL line compared to E_s . The correlation discussed in the previous paragraph, however, allows us to determine the splitting from the phase of the time-resolved PL pulses. Figure 5 depicts time-resolved PL traces recorded for detection energies ranging from the lower [1.5316 eV, Fig. 5(a)] to the higher [1.5339 eV, Fig. 5(k)] energy flanks of the PL line in Fig. 1(a) in steps of 0.25 meV. The signals collected for the two energy extrema peak at times $t_{\min} = 0.55 \text{ ns} + mT_{\text{SAW}}$ (solid vertical lines) and $t_{\max} = 1.51 \text{ ns} + mT_{\text{SAW}}$ (dashed vertical lines), where m is an integer. The peaks are displaced by $T_{\text{SAW}}/2$, in agreement with the calculations in Fig. 3. For

other energies, the PL phase varies between these two extremes. In Fig. 1(b), the spectral dependence of the PL intensity at times t_{\min} and t_{\max} is compared with the corresponding cw data. The energy separation $E_s = 1.4 \text{ meV}$ between the outer two peaks corresponds closely to the difference between the calculated transition energies at the positions of maximum and minimum band gaps, indicated by the dashed and solid arrows in Fig. 3(b), respectively. In agreement with the calculations, the peak at high energies exhibits a much larger oscillator strength. The latter explains the apparent blueshift of the cw PL line displayed in Fig. 1(a).⁵

Figure 1(b) shows an additional peak at the average energy $\bar{E}_g = (E_{g,\max} + E_{g,\min})/2$ (vertical arrow), for which the time-resolved traces in Fig. 5(e) display a strong modulation at the second harmonic of the SAW frequency. Although a $2\omega_{\text{SAW}}$ modulation is expected for detection at \bar{E}_g , the amplitude of the oscillations is considerably higher than that predicted in the simulations [cf. Fig. 3(c)]. The high modulation intensity is attributed to the vertical (i.e., perpendicular to the surface) component E_z of the SAW piezoelectric field, which has not been taken into account in the previous considerations. The quantum-confined Stark effect induced by E_z reduces the overlap between the electron and hole wave functions (and thus the oscillator strength) and, to a lesser extent, the recombination energy. For a Rayleigh SAW, E_z is shifted in phase by 90° with respect to the potential Φ and to the band-gap modulation. As a result, the energy shifts induced by E_z are the same for $E_{g,\max}$ and $E_{g,\min}$, so that the energy splitting E_s is not affected. E_z , however, vanishes close to \bar{E}_g , thus leading to the enhanced recombination observed in Fig. 5(e).

In conclusion, we have investigated the dynamic modulation of the band structure and of the carrier density induced by a SAW using spatially and time-resolved PL measurements. This technique allows for a direct mapping of the carrier densities and of the recombination energies. We demonstrate that the modulation of the electronic properties depends not only on the SAW acoustic and piezoelectric fields, but also on the transport properties of the carriers.

We thank H. Grahn for comments and for a critical reading of the manuscript. Support from the Deutsche Forschungsgemeinschaft (Project No. SA598/2-1) is gratefully acknowledged.

*Electronic address: falsina@pdi-berlin.de

¹K.S. Zhuravlev, D.P. Petrov, Yu.B. Bolkhovityanov, and N.S. Rudaja, *Appl. Phys. Lett.* **70**, 3389 (1997).

²C. Rocke, S. Zimmermann, A. Wixforth, J.P. Kotthaus, G. Böhm, and G. Weimann, *Phys. Rev. Lett.* **78**, 4099 (1997).

³P.V. Santos, M. Ramsteiner, and F. Jungnickel, *Appl. Phys. Lett.*

72, 2099 (1998).

⁴M. Hagn, A. Zrenner, G. Böhm, and G. Weimann, *Appl. Phys. Lett.* **767**, 232 (1995).

⁵T. Sogawa, P.V. Santos, S.K. Zhang, S. Eshlaghi, A.D. Wieck, and K.H. Ploog, *Phys. Rev. B* **63**, 121307 (2001).

⁶S. Simon, *Phys. Rev. B* **54**, 13878 (1996).